metals

MDPI

Article

Tool Downscaling Effects on the Friction Stir Spot Welding Process and Properties of Current-Carrying Welded Aluminum–Copper Joints for E-Mobility Applications

Aristide Tchouaha Tankoua [1,2,*], Tobias Köhler [2], Jean Pierre Bergmann [2], Michael Grätzel [2], Philip Betz [1] and Dirk Lindenau [1]

1 Planning and Production Technology, Mercedes-Benz AG, 70546 Stuttgart, Germany; philip.betz@daimler.com (P.B.); dirk.lindenau@daimler.com (D.L.)
2 Production Technology Group, Technische Universität Ilmenau, 98693 Ilmenau, Germany; tobias.koehler@tu-ilmenau.de (T.K.); jeanpierre.bergmann@tu-ilmenau.de (J.P.B.); michael.graetzel@tu-ilmenau.de (M.G.)
* Correspondence: aristide.tchouaha_tankoua@daimler.com

Citation: Tchouaha Tankoua, A.; Köhler, T.; Bergmann, J.P.; Grätzel, M.; Betz, P.; Lindenau, D. Tool Downscaling Effects on the Friction Stir Spot Welding Process and Properties of Current-Carrying Welded Aluminum–Copper Joints for E-Mobility Applications. *Metals* **2021**, *11*, 1949. https://doi.org/10.3390/met11121949

Academic Editor: Hoon-Hwe Cho

Received: 28 October 2021
Accepted: 26 November 2021
Published: 3 December 2021

Abstract: According to the technical breakthrough towards E-Mobility, current-carrying dissimilar joints between aluminum and copper are gaining an increasing relevance for the automotive industry and thus, coming into focus of many research activities. The joining of dissimilar material in general is well known to be a challenging task. Furthermore, the current-carrying joining components in E-Drive consist of pure aluminum and copper materials with relatively thin sheet thickness, which are thermally and mechanically very sensitive, as well as highly heat and electrically conductive. This results in additional challenges for the joining process. Due to their properties, friction stir welding and especially fiction stir spot welding (FSSW) using pinless tools—i.e., as hybrid friction diffusion bonding process (HFDB) is more and more attractive for new application fields and particularly promising for aluminum–copper joining tasks in E-Mobility. However, the feasibility is restricted because of the relatively high process forces required during friction stir welding. Thus, to fulfill the high process and quality requirements in this above-mentioned application field, further research and process development towards process force reduction are necessary. This work deals with the application of the tool downscaling strategy as a mean of process force reduction in FSSW of thin aluminum and copper sheets for current-carrying applications in E-Mobility, where the components are very sensitive to high mechanical loads. The tool downscaling approach enables constant weld quality in similar process time of about 0.5 s despite reduced process forces and torques. By reducing the tool diameter from 10 mm to 6 mm, the process force could be reduced by 36% and the torque by over 50%. Furthermore, a similar heat propagation behavior in the component is observable. These results provide a good basis for the joining of E-Drive components with thermal and mechanical sensitive sheet materials using the pinless FSSW process.

Keywords: friction stir spot welding; FSSW; HFDB; process force reduction; tool downscaling; dissimilar joints; aluminum–copper; thin sheets; E-Mobility

1. Introduction

Energy efficiency and especially environmental friendliness as well as the reduction of CO_2 emissions are new challenges in the development of future vehicles, since the requirements regarding the emission of CO_2 and other greenhouse gases are getting more and more higher. Aerodynamic and lightweight approaches are not sufficient anymore to satisfy these high environmental requirements and thus actions on drive level must be pursued. This approach is also corroborated and supported by governments [1,2] and the European Union [3] as well and leading to the technological trend towards E-Mobility. However, to exhaust the full potential of E-Mobility, research and development activities must be carried out at different levels. Especially regarding joining technologies, the E-Mobility trend is combined with new challenges for the automotive industry. This is due to new components, materials and their combinations in E-Drive among others.

The joining of aluminum with copper on battery module level in particular is a very challenging task, which requires precise process development. The challenges reside in different aspects—electrical, thermal, metallurgical and mechanical [4–7]. Due to different thermo-physical properties, the joining of dissimilar materials is commonly not trivial. The copper and aluminum materials in the E-Drive components are high conductive pure materials with low sheet thicknesses, high thermal and mechanical sensitivity, which makes the joining task additionally complex [4–7]. To achieve joints with low electrical resistance (i.e., high electrical performance), the part should be joined by means of material bonding methods [5]. Mechanical processes such as clinching [8] and especially bolting [9], provide joints with higher electrical resistance due to the constriction resistance areas resulting. Furthermore, additional weight can be caused while using fasteners [4,7,10]. The use of conventional fusion welding process such as arc welding, resistance spot welding is just hardly possible because of the difference in the material properties of the joining parts, e.g., the different melting temperatures and the thermal expansion.

By means of innovative technologies such as laser beam welding (LBW), the highly conductive pure aluminum and copper materials in E-Drive components can be joined. The short process time, the high precision and thus, the suitability for micro applications make the contactless LBW process an established method for battery module manufacturing [4,6,7,10–12]. However, undesired brittle and intermetallic compounds (IMCs) with higher electrical resistances can occur during the process [4,7,10,13–15]. Furthermore, the LBW process is very sensitive to gaps between the overlapped welding parts (the so-called zero-gap problematic) and other tolerance inaccuracies [15–17]. These aspects lead to many challenges and instabilities in the mass production of laser welded current-carrying Al–Cu E-Drive components. Thus, in order to overcome these mentioned negative aspects, solid-state welding processes, such as ultrasonic welding [4,5,7,10,18,19] or especially friction stir welding are ideal candidates to achieve this joining task [20–26]. However, further process developments are needed to exploit the high potential of these innovative technologies.

Contrary to ultrasonic welding, FSW is not mentioned in the recent reviews as a joining method for the manufacturing of current-carrying components in E-Drive [4–7,10]. Instead, friction stir welding resides in focus of many recent works around dissimilar Al–Cu joints [22,23,25,27–31]. Apart from the conventional friction stir welding (path process variant), there are further process variants such as refill fiction stir spot welding [32–34] which is developed to replace resistance spot welding in car body applications as well as the classical friction stir spot welding, [20,35–40], which are very promising. The above-mentioned process variant—friction stir spot welding (FSSW)—is especially attractive because of the easier handling, clamping and the lower process time compared to the path process variant. Furthermore, the occurring eutectic reaction in the aluminum–copper interface during the FSSW process enables welds in relatively low process time as shown by Roos [41]. As mentioned above, the aluminum and copper materials in the current-carrying E-Drive components are pure materials, which are thermally and mechanically sensitive. Consequently, low mechanical loads are crucial in such applications. In general, the required energy in FSSW processes is generated by relatively high tool rotational speeds and process forces, whereby the last-mentioned must be reduced for battery applications. Therefore, it is necessary to keep the welding forces at a minimum to achieve a high process stability and constant joint properties. Furthermore, the choice of these major process parameters (force and rotational speed) depend on the tool dimension.

An approach for process force reduction by means of targeted reducing of both tool shoulder and pin dimension during friction stir (path) welding is presented in the work of Regensburg et al. [42]. This tool downscaling approach ensures approximately constant mechanical weld properties while reducing the tool diameters and thus, the process forces. The process force reduction also enables the reduction of the clamping devices as well as the welding system as a whole. Another benefit of tool downscaling approach is the weldability of workpieces with restricted accessibility. The approach is pursued and thoroughly investigated in the works of Grätzel et al. [43–45], where the potential of tool scaling in friction stir (path) welding of aluminum alloys for example in heat exchanger applications is shown [43].

Unlike the above-mentioned works, this paper focuses on the friction stir spot process with pinless tools and relatively low plunging depth. In this process variant—also known as hybrid friction diffusion bonding (HFDB) [41]—the overlapped welding parts are bonded via diffusion mechanisms without significant cross section reduction. This is particularly relevant, while manufacturing current-carrying welds with thin sheets, whose joint performance is highly dependent on the material thickness. Furthermore, this work addresses the manufacturing of aluminum–copper dissimilar joints while combining the above-described process specifications, pure materials with sheet thickness $\leq$ 1 mm and the process force reduction by means of the tool scaling approach. These aspects have not yet been investigated. Furthermore, apart from the transferability of the tool downscaling approach on FSSW, which is not investigated in previous works, the application on dissimilar joints and especially Al–Cu-joints, the heat propagation during the process as well as the limits of this approach regarding heat input and joints performance are thematically focused in this study. Moreover, this work also addresses the influence of the tool downscaling approach on the mechanical and electrical weld properties, so that effects of the process force reduction by mean of tool downscaling can be investigated holistically with process-technical conditions and application-specific joint properties.

In contrast to the HFDB process, which is mainly determined by friction and diffusion subphenomena, while joining aluminum with copper by mean of pinless FSSW, the eutectic melt phenomenon contributes significantly to the weld formation. This process variant presented in the work of Regensburg [46] is therefore designated as hybrid friction eutectic bonding (HFEB). The process curves of such a process are depicted in Figure 1. The upper diagram (Figure 1a) shows the process force and rotational speed over the time, whereas the curves of the resulting process torque and plunging depth over the process time are shown in the diagram bottom (Figure 1b).

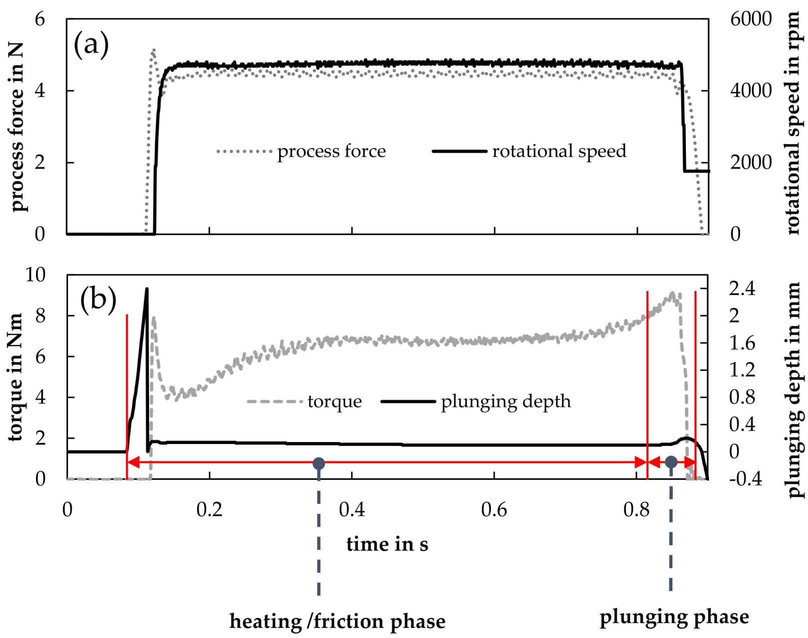

Figure 1. Process diagrams—process force and speed over time (**a**) as well as process torque and plunging depth over the time (**b**).

Because of the contact establishment between the welding tool and the welding parts at the beginning of the process, peaks are recognizable in the force and plunging depth curves in the friction phase. After reaching the sliding friction (overcoming the static friction) as it can be seen in Figure 1 according to the peak in the torque diagram, the rotational speed start increasing, and the defined process parameter are set by the machine. As mentioned above the tool do not penetrate the welding part. Instead, because of the thermal expansion, the welding tool is slightly pushed away from the welding parts until the start of the plunging phase, which compare to the heating phase is very short. From the beginning of the plunging phase, the torque increases until its maximum upon reaching the defined plunging depth.

2. Materials and Methods

The achieved experiments in the scope of this work have been carried out using an EJOWELD friction element welding setup EJOT RES 38/155 RRS C2 (EJOT GmbH & Co. KG, Tambach-Dietharz, Germany), which has been modified and adjusted for the friction stir spot welding process by "Ilmenauer Fertigungstechnik" at the Technische Universität Ilmenau. The welding process was force controlled to ensure a constant surface pressurization during the process. The setup allows welding forces up to 6 kN and rotational speeds up to 8000 rpm. The welding parts are hold by an anvil, which is attached to the C-Frame so that a closed force flow can be achieved. During the process, the welding parts were held down by a cylindrical down holder, which surrounds the welding tool and stabilizes the welding parts. To avoid a large end crater and cross section reduction, pinless welding tools made of the hot-working steel X40CrMoV5-1 (1.2344) from the manufacturer Stauber (Stauber GmbH, Meckesheim, Germany) were used. Thus, the used tools with a cylindrical shape consist of a flat shoulder, which generates heat while rotating and simultaneously pressurizing the upper surface of the welding part. The welding setup and the used tool geometry are depicted in Figure 2. A tool with 10 mm diameter was used as reference and two further tools with respectively 8 mm and 6 mm diameters were tested to observe the effects of the tool diameter reduction on the process behavior and on the resulting weld properties as well.

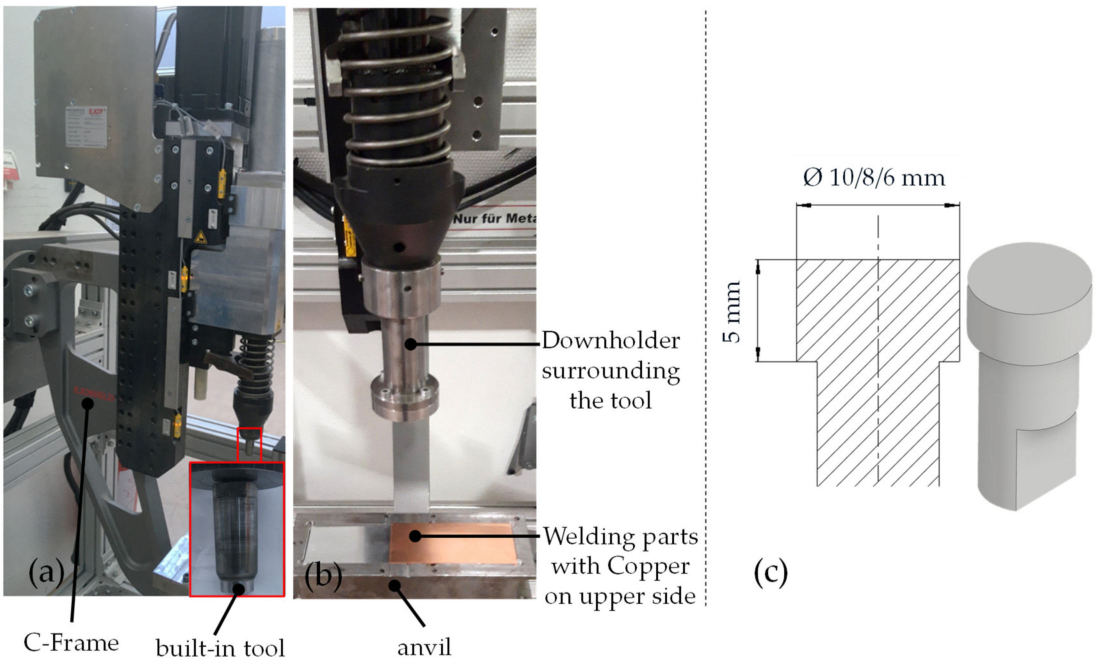

Figure 2. Welding setup with included welding parts (**a**,**b**) and geometry of the used pinless tools (**c**).

The welding parts consists of pure aluminum EN AW 1070 (Norsk Hydro ASA, Oslo, Norway) and pure copper EN CW 024A (Ferd. Haecker KG, Pforzheim, Germany) with sheets thicknesses of respectively 1 mm and 0.7 mm. These were ordered in an overlap configuration with 35 mm overlap length according to DIN EN ISO 14273 [47] (cf. Figure 3).

Therefore, the copper sheet overlaps the aluminum sheet so that a better conduction of the generated heat from the copper upper surface to the Al–Cu interface is possible. Reversing the arrangement could lead to aluminum melting, which has a significantly lower melting temperature (approx. 660 °C) than copper (1085 °C), without weld formation. Figure 3 also shows a section of a weld with marked position and shape of samples for metallographic analysis.

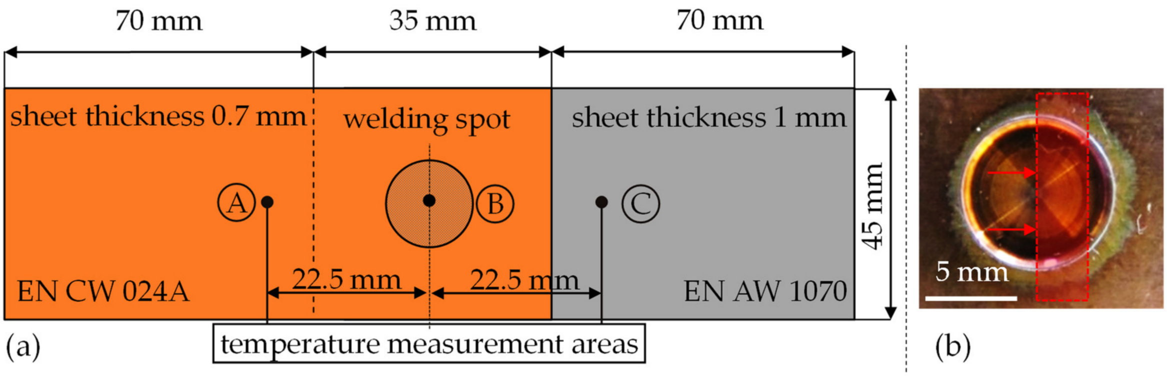

Figure 3. Geometry and configuration of the weld specimens with temperature measurement areas (**a**) and weld cut-out with marked section region for metallographic sample (**b**). The measurement areas for the temperature were at the Al–Cu-interface (B), at a distance of 22.5 mm from the welding spot middle in copper (A) and aluminum (C).

Different parameter sets were defined for the reference tool (10 mm diameter) - each consisting of variable force, rotational speed and the constant plunging depth. Each three variations of process forces (3000 N, 4500 N and 6000 N) and rotational speeds (4000 rpm, 4800 rpm, 7000 rpm) were tested with the reference tool to evaluate the influence of different induced surface pressures and tool circumferential speeds on the process and on the weld quality. These parameters (force and rotational speed) were scaled down on the further tool dimensions as shown in Figure 4. The resulting parameter matrix with the different parameter sets is presented in Table 1. For statistical repeatability, three tests were performed per parameter set.

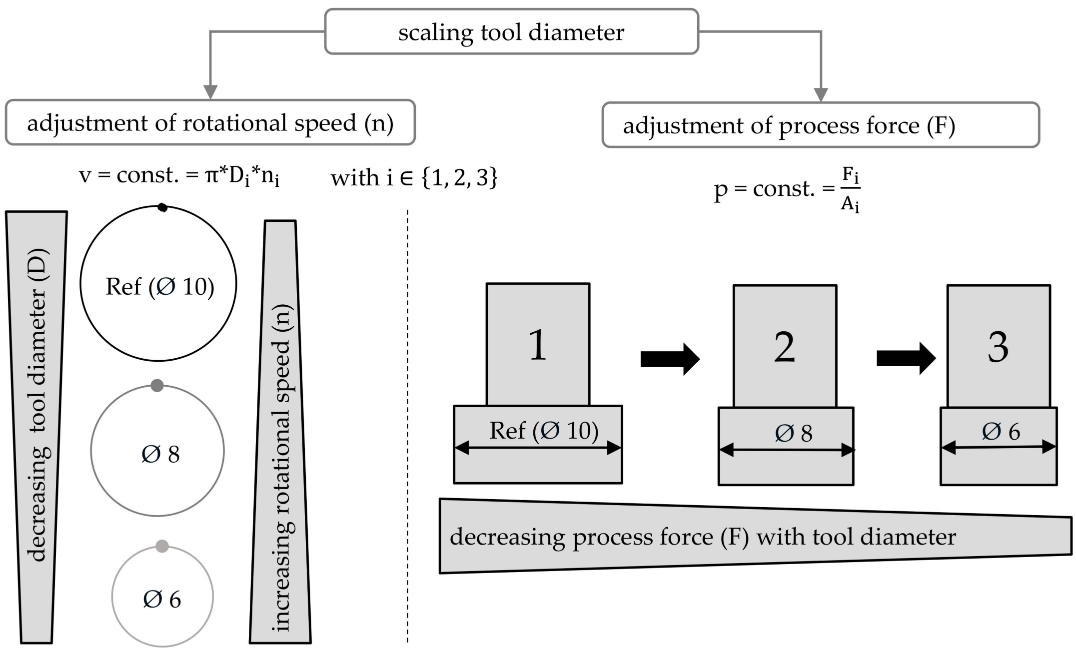

Figure 4. Tool downscaling strategy with constant circumferential speed (v) and surface pressure (p).

Table 1. Parameter matrix with three levels of circumferential speeds and surface pressures, which were held constant for all tools diameters and each corresponding respectively to a rotational speed and process force according to the tool scaling level.

Used Constants		**Tool Downscaling**		
Tool diameter		10 mm (Ref.)	8 mm	6 mm
Circumferential speed/rotational speed:	2094.4 mm/min 2513.3 mm/min 2932.2 mm/min	4000 rpm 4800 rpm 5600 rpm	5000 rpm 6000 rpm 7000 rpm	6666 rpm 8000 rpm 9333 rpm *
Surface pressure/process force	38.2 N/mm^2 57.3 N/mm^2 76.4 N/mm^2	3.0 kN 4.5 kN 6.0 kN	1.92 kN 2.88 kN 3.84 kN	1.08 kN 1.62 kN 2.16 kN
Plunging depth		0.2 mm		

* max. machine rotational speed of 8000 rpm exceeded.

For the metallurgical, mechanical and electrical characterization of the manufactured welds, proper test methods were used, respectively. The welds were metallographically analyzed using a Zeiss Axio Vision light microscope (Carl Zeiss AG, Oberkochen, Germany) following a metallographic preparation of the samples. The mechanical properties were evaluated in a shear tensile test using a Zwick/Roell test system (Zwick Roell GmbH & Co. KG, Ulm, Germany) at a testing velocity of 10 mm/min, whereas the electrical tests were performed with a four-wire resistance measurement setup. The above-mentioned consists of a Gossen Metrawatt Single-Output System Power Supply SSP 240-20 (Gossen Metrawatt GmbH, Nürnberg, Germany) and a nanovoltmeter 2182A from Keithley Instruments/Tektronix (Tektronix GmbH, Köln, Germany), which provides high accurate results with an impedance of over 10 GΩ [48]. Apart from the temperature measurement at the Al–Cu weld interface, further temperature measurement areas were set at the points "A" und "C" to investigate the heat propagation during the process (cf. Figure 3). In the further course of this paper, the above-mentioned two measurement areas are also referred to "Temp. Cu" and "Temp Al" respectively. The temperature measurement was carried out using thermocouples type K. The results of the different investigations in the scope of this work are shown in the next section.

3. Results and Discussion

3.1. Influence of the Welding Parameters Force and Rotational Speed on the Process Behavior

To understand the effects of the welding process parameters, investigations with the reference tool—i.e., 10 mm diameter were realized with different levels of forces and rotational speeds. This leads to different process times and heat propagation behavior in the welding parts. The process time corresponds to the time from the first contact of the tool with the welding parts until the retracting after reaching the plunging depth of 0.2 mm. The results are shown in Figure 5, where the rotational speeds and the process forces are converted into the resulting circumferential speeds and surface pressures respectively (cf. Table 1). The diagrams are sectioned in three quadrants (I, II, III), corresponding to the different levels of process forces and thus, surface pressures. In each quadrant, the three investigated circumferential speeds are considered. The number of the samples is given as "$n = 3$" in the dashed square marker. This indication is analogously used in the further diagrams in this work to specify the amount of the tested samples. The upper diagram (a) shows that the welding process time decreases with higher rotational speed in all quadrants (at all process force levels). This is due to the higher heating rate and the combined reduction of the heating phase duration, which represents the highest proportion of the whole process time.

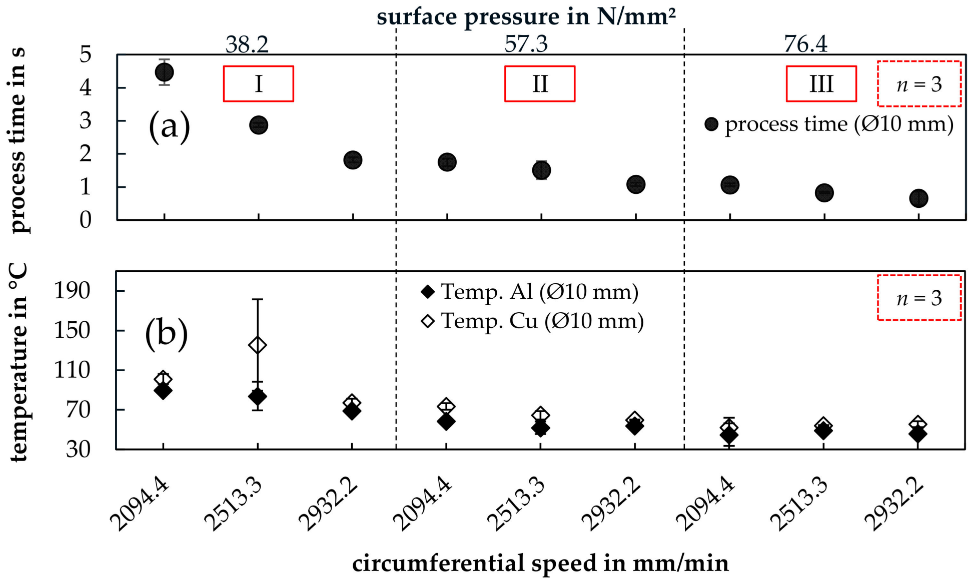

Figure 5. Influence of the welding process parameters on the process time (**a**) and heat propagation (**b**).

Especially at lower process forces and respectively lower surface pressure in the first quadrant, this effect is more pronounced, and the process time decreases up to ~60% from 4.47 ± 0.39 to 1.82 ± 0.08 s. The relatively high standard deviation in the first quadrant at 2513.3 mm/min is due to irregularities during the experiments. In the quadrants II and III, the process time decreases with a flatter tendency. While considering a constant circumferential speed at the three pressures levels, it is obvious that the process time is also decreasing with higher surface pressure—that means higher process forces. The lowest process time was achieved in the third quadrant in the diagram at 2932.2 mm/min (5600 rpm) and 76.4 N/mm^2 (6 kN). In total, it can be noted that higher rotational speeds combined with higher process forces result in a process acceleration. Additionally, according to the bottom diagram (b), the reached maximum temperatures in the measuring points "Temp. Cu" and "Temp. Al", representing the thermal sensitive areas "A" and "C" (cf. Figure 3) are following the same tendency and decrease with the process time at higher process forces and rotational speeds as well—i.e., at higher contact pressures and circumferential speeds respectively. The correlation of shorter process time with lower heat propagation can be explained by the close relationship between these two parameters during the HFDB process, as shown in the work of Roos [41]. According to his work, the process temperature, the process time and surface pressure are closely related. These parameters determine both the HFDB process and the joint properties. He showed that by increasing the surface pressure while joining aluminum with steel, the process time and process temperature in the welding area could be reduced. However, the propagation of the generated heat and the temperature distribution outside the welding area, along the joining partners were not considered. Rather, Ross described the time-dependent aspect of frictional heat and process temperature during the HFDB process. Thus, the reduced heat propagation can logically be explained by the shorter process time. As shown in Figure 6, the temperature at the Al–Cu-interface in the welding spot—i.e., measurement area "B" (cf. Figure 3) was around 550 °C for all parameter sets—corresponding to the eutectic temperature in the Al–Cu-system.

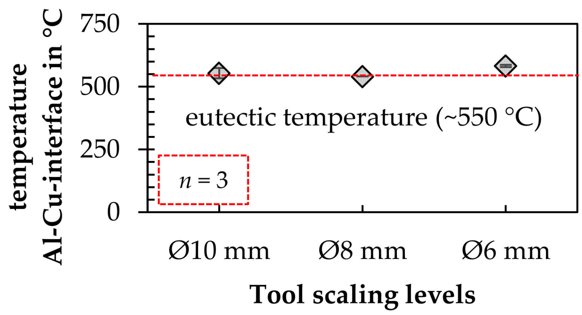

Figure 6. Process temperature at the Al–Cu weld interface for the different tool scaling levels at 2513.3 mm/min circumferential speed and 57.3 N/mm^2 surface pressure.

Concerning the occurring mechanical loads on the welding parts, the maximum torque resulting from the process was recorded. The results are depicted in Figure 7. This shows that the rotational speed does not significantly affect the maximum torque occurring during the process. The change in the maximum torque while increasing the circumferential speed from its lowest level of 2094.4 mm/mm (4000 rpm) to its highest level of 2932.2 mm/min (5600 rpm) in the second quadrant in the diagram is about 8% and in the first and third quadrant less than 2%. However, there is no clear tendency of increasing or decreasing torque with increasing circumferential or rotational speed discernible, so that the maximum torque occurring during the process can be assumed as nearly constant regardless the rotational speed levels. In contrast, an increase of the maximum torque with higher process forces is obviously recognizable. While increasing the surface pressure from 38.2 N/mm^2 (3 kN) in the first to 76.4 N/mm^2 (6 kN) in the third quadrant, the maximum torque increases by over 40%.

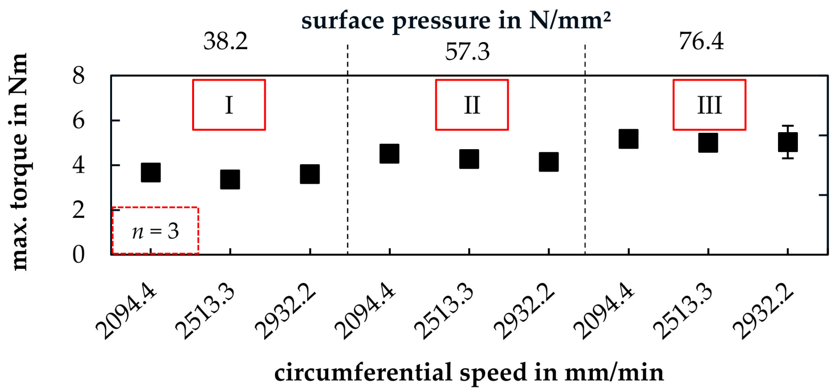

Figure 7. Influence of the welding process parameters on the occurring maximum torque—used tool (Ø10 mm).

Since on the one hand, higher surface pressures induced by respectively higher process forces are favorable for shorter process time and low thermal loads, as shown above, it is necessary to reduce the process forces to avoid high torque and thus, eventual damages on the welding parts during the process. However, the process force reduction ideally should not affect the surface pressure, which ensures the above-mentioned process-technical benefits. This solution measure requires contact surface reduction, which resides in the tool diameter scaling approach pursued in this work. After considering the effects of the welding parameters on the process in this section, the properties on the achieved welds at the different parameters are contrasted in the following.

3.2. Influence of Welding Parameters Force and Rotational Speed on the Weld Properties

For the influence of process parameters on the weld quality, the metallographic aspect is first considered. A typical microsection of the weld is exemplarily shown in (Figure 8), where the Al–Cu interface and its metallographic constitution is described. This consists of the θ-Phase (Al_2Cu) with dendritic shape in the eutectic melt matrix, the eutectic matrix and α-aluminum precipitations. The occurring intermetallic compounds are the least critical in the Al–Cu-System regarding electrical properties and brittleness [14].

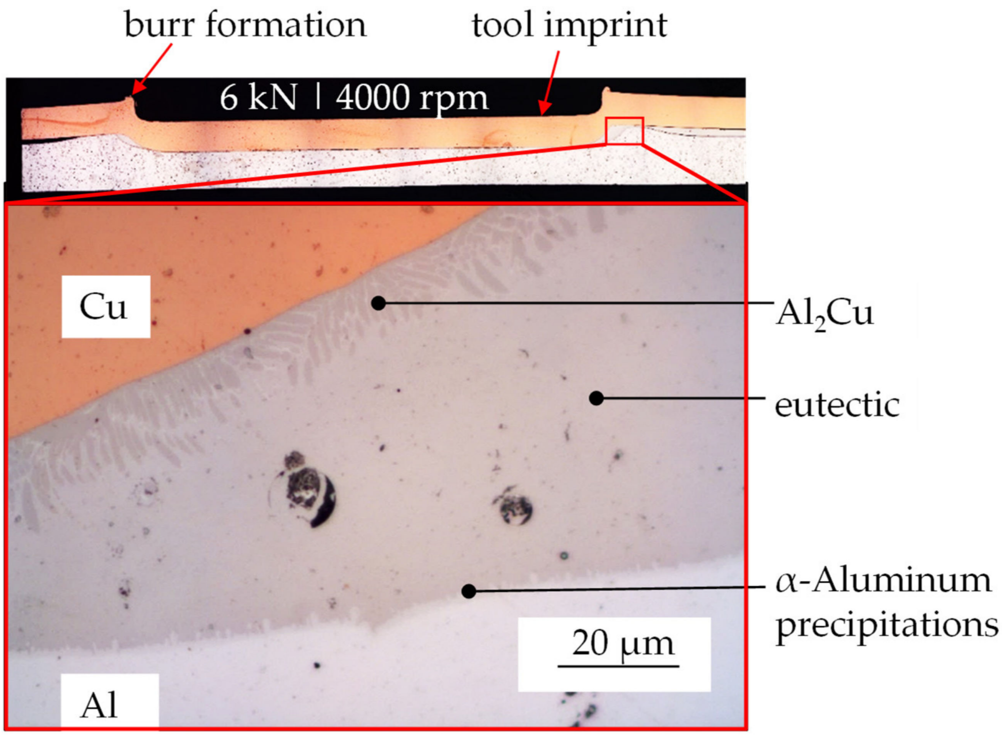

Figure 8. Microsection of a weld with its typical metallographic constitution exemplary—used tool (Ø10 mm).

Depending on the welding parameters, the solidification of the eutectic melt can be either accelerated or slowed down and thus, impacting the weld constitution and quality as discussed by Regensburg et al. [31]. An important aspect is to obtain pore-free welds and thus, avoiding a weakening of the cross-sectional area and a deterioration of the physical properties, in particular the electrical conductivity. Figure 9 shows that the pore formation can be reduced at higher process forces and decreases with process time. At a higher process force of 6 kN (76.4 N/mm^2) pore-free welds could be achieved within an average process time of 0.62 s. At a moderated force level i.e., 4.5 kN (57.3 N/mm^2) the microsection shows correspondingly moderated pore formation in the weld and the process time was 1.75 s. Among the analyzed process forces, the highest pore formation was achieved at 3 kN (38.2 N/mm^2), where the highest process time of 4.47 s was reached as well. This effect of decreasing pore formation with higher process forces can be explained on the one hand by the faster surface approach at the Al–Cu interface leading to a faster eutectic melt formation, as a result of higher surface pressures generated by higher process forces. On the other hand, higher process times lead to a eutectic melt formation with a higher amount of aluminum, which solidifies slowly and favors the pore formation as well.

Regarding the influence of the rotational speed, it is worth mentioning prior that the rotational speed basically has a high influence on the generated heat during the friction stir welding process. This is shown in the investigations of Schmid, where the influence of the different welding parameter on the diffusion mechanism and thus, on the process be-havior are discussed [49].

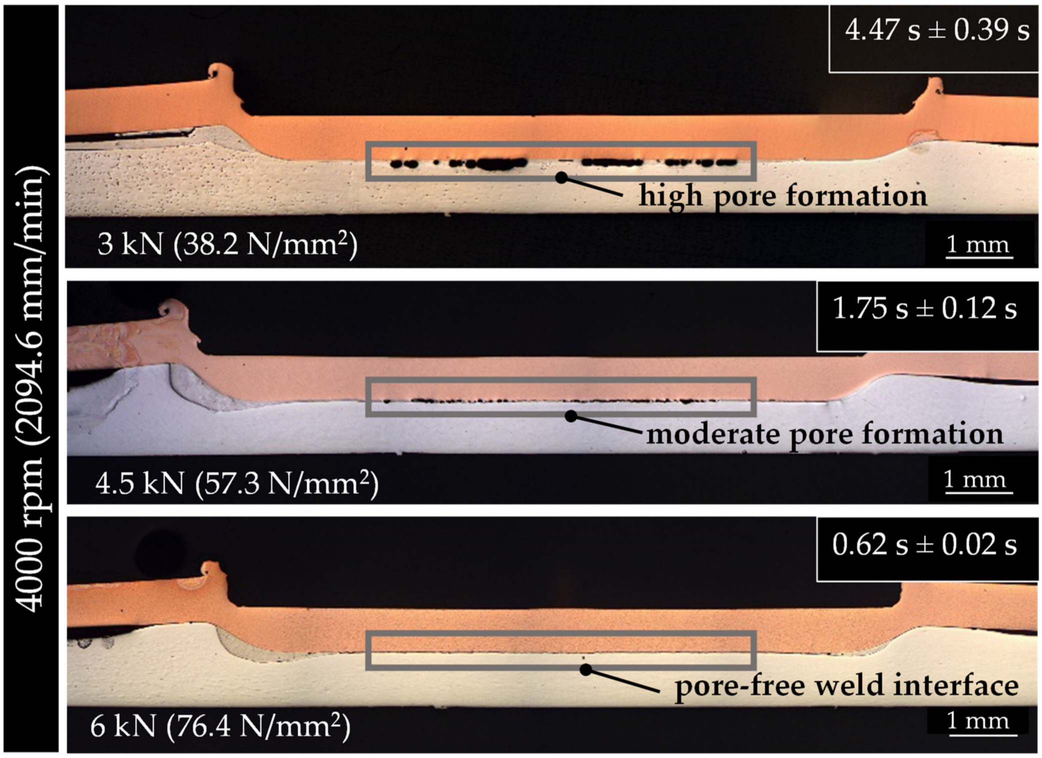

Figure 9. Metallographic micrographs of welds at constant rotational speed and different welding process forces—higher process forces lead to lower process times and pore-free welds—used tool (Ø10 mm).

The effects of rotational speed on the weld are illustrated in Figure 10, where welds achieved with a constant process force 3 kN (38.2 N/mm^2) and three different rotational speeds are shown. At the highest level—i.e., 8000 rpm (2932.2 mm/min) with an average process time of 1 s, multiple and large pores are visible in the weld microsection. The increasing pore formation in the weld interface despite decreasing process time can be explained by the generated heat amount and the constitution of the resulting eutectic melt. Higher heat rates induce short process times and can lead to aluminum-richer eutectic melt formation, which is combined with an abrupt decrease of the solubility of hydrogen in aluminum and thus, resulting in the formation of many and large pores in the weld interface. These aspects are thoroughly discussed in the work of Regensburg et al. [31]. Furthermore, a pronounced pore formation in correlation with higher process times (4.47 s) at lower rotational speed—i.e., 4000 rpm could be also observed in the weld interface. Welds with moderate pore formation could be achieved with a rotational speed of 6000 rpm (2513.3 mm/min) within a process time of 1.7 s.

In the following, to analyze the influence of the process parameters on the mechanical properties, failure loads, force-path curves and failure patterns of the tested samples are focused. Figure 11 obviously shows that the process parameters—especially process forces and respectively surface pressure do not significantly affect the failure loads, which is nearly constant for all parameter sets. Furthermore, also the pore formation especially at the Al–Cu weld interface do not influence the failure loads. The average failure load considering the standard deviation amounts to ~1600 N for all samples.

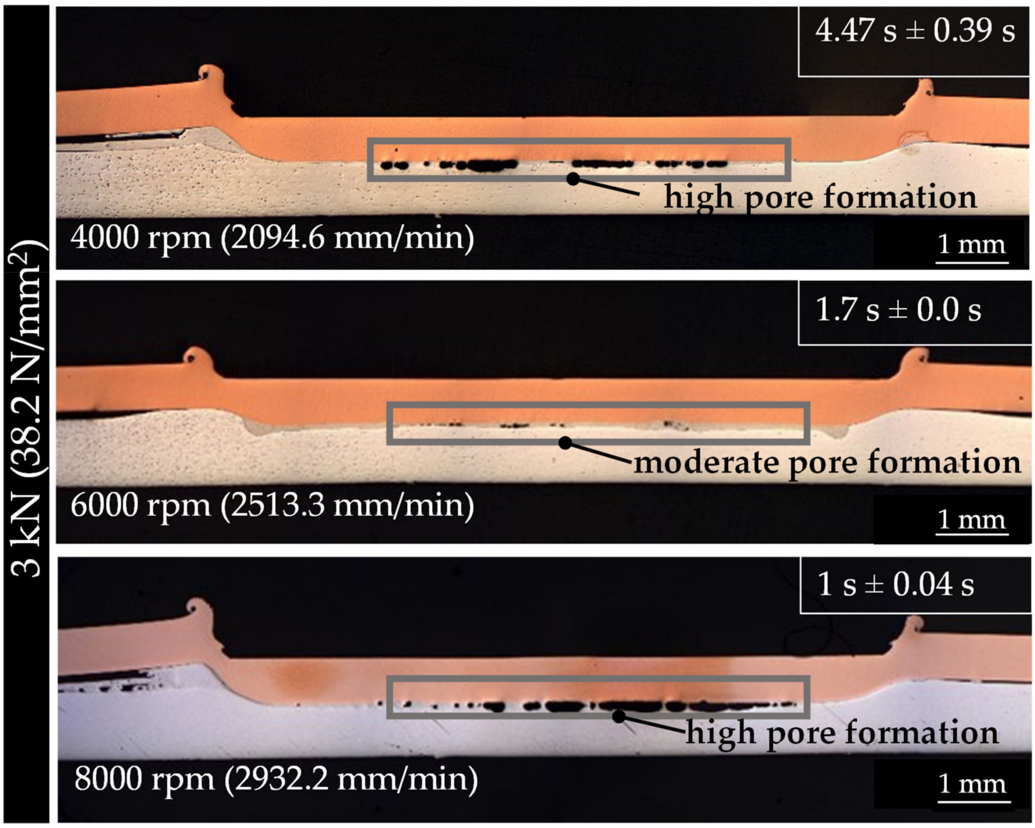

Figure 10. Metallographic micrographs of welds at constant process force and different rotational speeds. High pore formation at both lower and higher rotational speeds. Relatively lower pore formation at moderate rotational speeds—used tool (Ø10 mm).

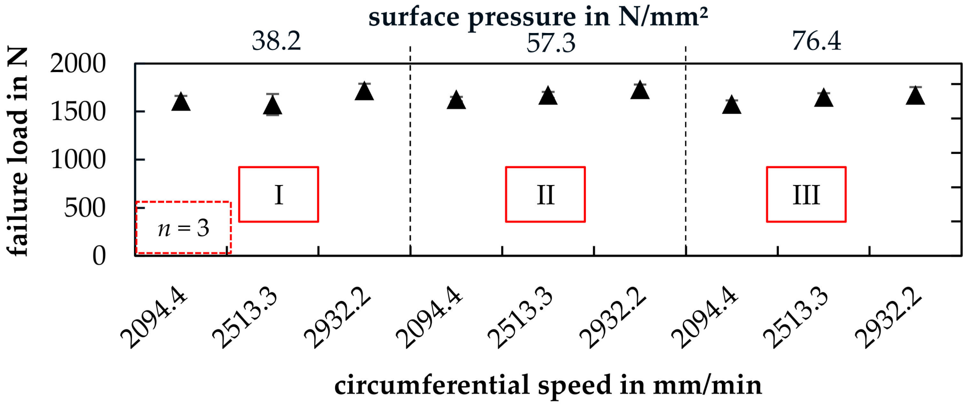

Figure 11. Influence of the process parameters on the failure loads—used tool (Ø10 mm).

Rather the rotational speed slightly affects the failure loads—an increasing tendency of the failure loads at higher circumferential speeds is recognizable. This tendency is also visible in the force-traverse path diagrams in Figures 12 and 13 respectively. According to the Figure 12, higher rotational speeds lead to an increase of both—maximum shear tensile forces (failure loads) and maximum traverse path. This can be explained by the increase of the spread eutectic melt width, which leads to a wider joint area overall, as shown in the work of Regensburg [46].

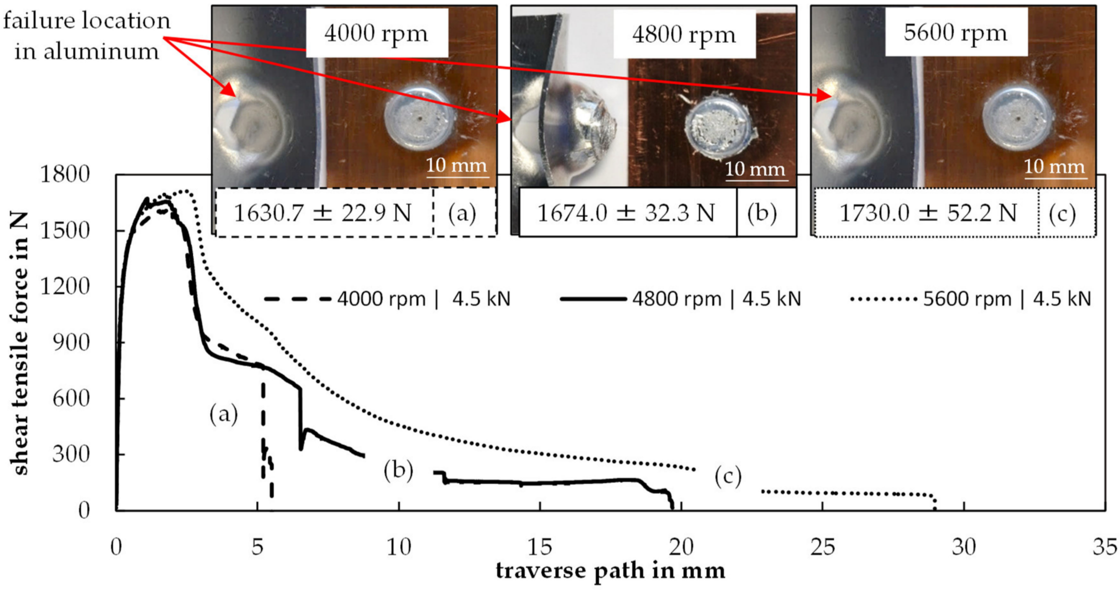

Figure 12. Influence of rotational speed on the force-path curves and failure patterns of the welded samples.

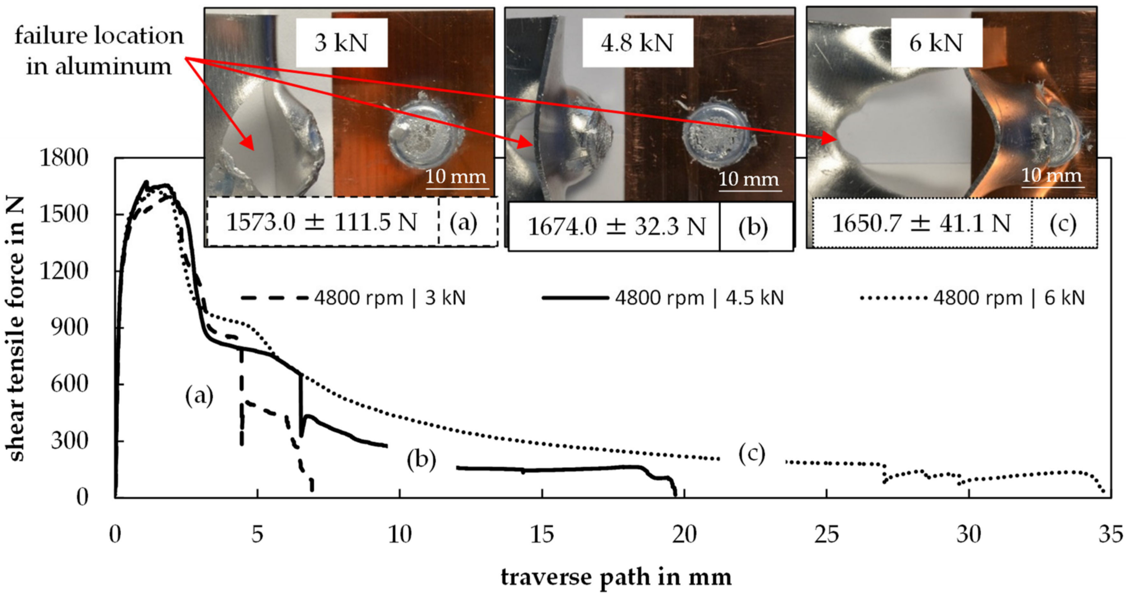

Figure 13. Influence of process force on the force-path curves and failure patterns of the welded samples.

On the other hand, even though the shear tensile forces regardless the welding force level remain unchanged, the maximum traverse path is also increasing with higher process forces (cf. Figure 13). However, the reached path at the maximum shear tensile force (failure load) coincide for all tool diameters and parameter sets. Furthermore, the inserted failure pattern in force-path diagram below (Figures 12 and 13) can explain the nearly constant failure load. Since all samples regardless the different parameter sets fail initially in the aluminum-based material, there is no significant difference between the shear tensile forces to be observed.

3.3. Effects of the Tool Downscaling on the Process Behavior

In this section, the results of the tool downscaling will be presented and discussed. As described above (cf. Section 2.), the used parameter sets based on the tool with 10 mm diameter were scaled on two other tool diameters (8 mm and 6 mm) while keeping the circumferential speed and the surface pressure constant. This requires a reduction of the process forces on the one hand, as well as an increase of the rotational speed on the other hand, as shown in Figure 14.

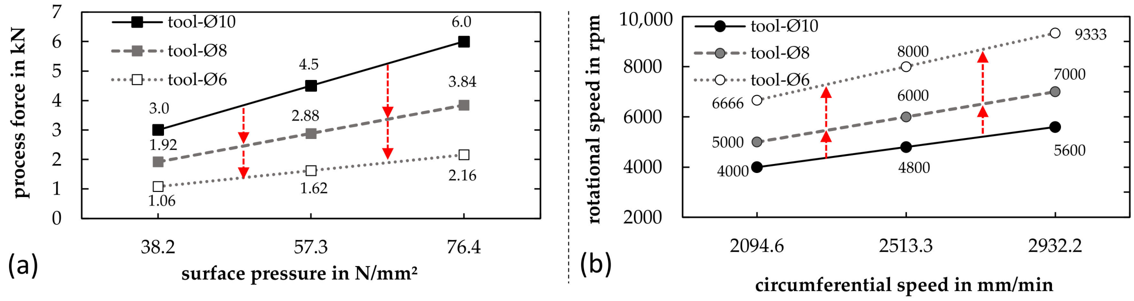

Figure 14. Tool diameter scaling approach—scaling of process forces (**a**) and rotational speed (**b**) with respect of constant surface pressure and circumferential speed.

The effects of reduced tool diameters on the process behavior are discussed in the following. The diagrams in Figure 15 are sectioned in three quadrants corresponding to the three used surface pressures—analogous to the diagram in Figure 5. In the first quadrant, at lowest surface pressure level (38.2 N/mm^2), welds could not be achieved with the 6 mm tool diameter—regardless of the circumferential speed. Moreover, due to the machine restrictions especially regarding the maximum rotational speed, tests at the highest circumferential speed level of (2932.2 mm/min (cf. Table 1)) could not be carried out with this smaller tool diameter. The upper diagram in Figure 15 shows the process time over the different circumferential speeds, whereas the bottom diagram depicts the maximum temperatures in the measurement area in aluminum (Temp. Al) corresponding to the area "C" in Figure 3. Since it has been shown in Section 3.1 that the temperatures in the two measuring areas "Temp. Al" and "Temp. Cu" are in the same range, only the temperature "Temp. Al" in the area "C" is considered representatively in this section to analyze the effects of the tool downscaling on the heat propagation during the process. According to the upper diagram in Figure 15, the same tendency of decreasing process time with higher surface pressures and circumferential speeds observed with the reference tool is recognizable for all tool diameters and parameter sets. Moreover, the correlation between low heat propagation—i.e., lower temperatures at the defined measurement points and the shorter process time is also recognizable according to the dashed circle markers in the diagrams.

This is especially obvious in the last two quadrants of the diagrams—that means at 57.3 and 76.4 N/mm^2. In these two quadrants, at 2513.3 mm/min circumferential speed, both—the process times and the temperatures "temp. Al" are nearly coinciding for all tool diameters (cf. Figure 15).

Additionally, regarding the mechanical loads occurring during the joining process, the same tendency observed with the reference tool diameter (10 mm) is visible with all other tool diameters (cf. Figure 16). The torque increases with higher surface pressure (process force), whereas this is nearly constant regardless the circumferential speeds. Based on these aspects—together with the above discussed effect on the temperature propagation, it can be stated that similar process conditions can be reached, while scaling down the tool diameter and compensating the welding forces and rotational speeds.

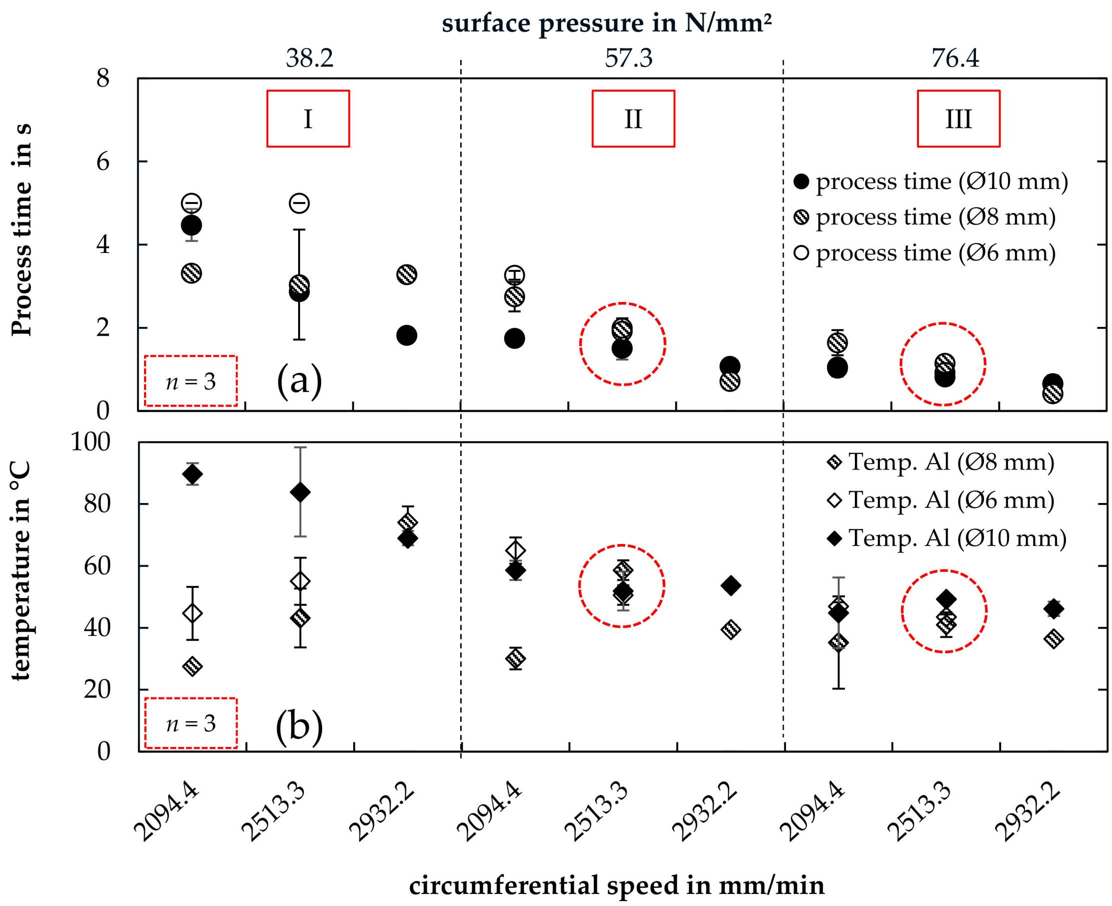

Figure 15. Effects of tool downscaling on the process time (**a**) and heat propagation (**b**).

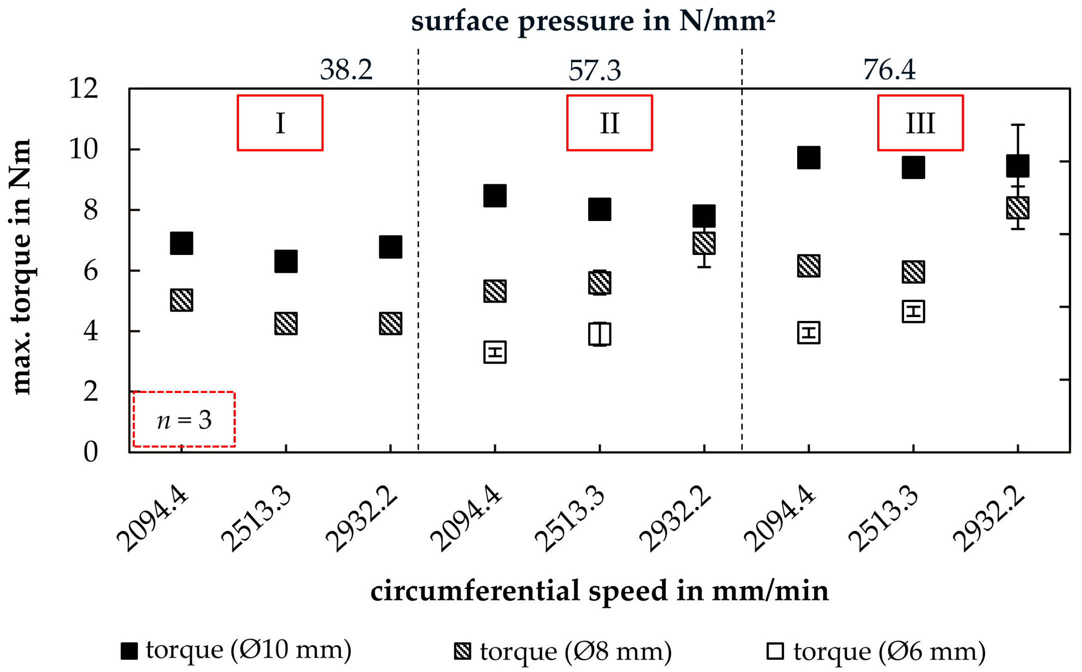

Figure 16. Effects of tool downscaling on the resulting maximum torque.

3.4. Effects of the Tool Downscaling on the Weld Properties

The effect of reduced tool diameter and thus, welding process forces on the weld quality—especially mechanical and metallurgical properties are discussed in this subsection. As it can be gathered from Figure 17, the failure loads decrease with smaller tool diameter regardless the used welding process parameters. On the one hand, this was to be expected since the weld area decreases with the tool diameter. On the other hand, this effect seems to be in contrast with the results of Grätzel et al. [44], where the failure loads could be kept constant despite the reduced tool diameter until −30%. However, the investigation of Grätzel were based on friction stir welding (FSW) of butt joints, which do not require large tool diameters to satisfy the mechanical weld requirements, as long as the gap bridge is ensured, and the used process parameters are suitable. Therefore, these results cannot be contrasted with the above-mentioned results properly.

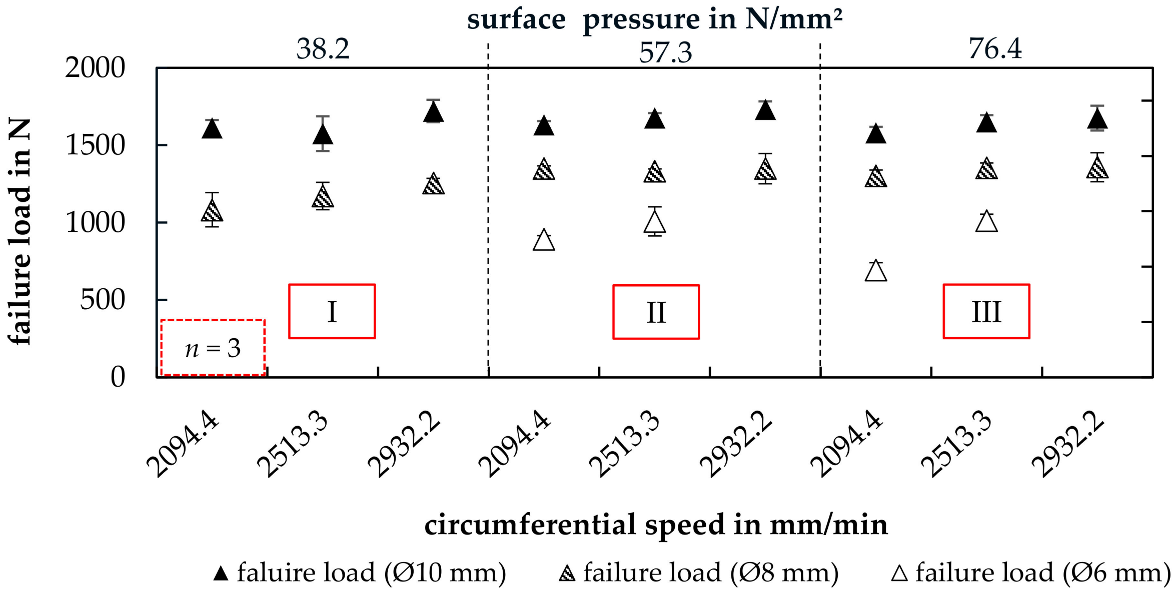

Figure 17. Effects of tool downscaling on the failure loads.

Focusing the second quadrant in the diagram—that means at a surface pressure of 57.3 N/mm^2, welds achieved with 10 mm tool diameter fail averagely at 1650 N, whereas specimens welded with the 8 mm tool fail at 1340 N. The lowest shear tensile failure loads of averagely 1200 N were recorded for joints welded with the 6 mm diameter tool.

Furthermore, according to the failure pattern in Figure 18, although the welds fail in the aluminum-based material initially, the overall failure behavior involves the joining area. This is also visible in the curves, which do not progress smooth after the max. shear tensile force is reached. The involvement of the weld area in the failure behavior justifies the effects of decreasing failure load with smaller tool diameters. Furthermore, regarding the traverse path, the following force-path diagrams show that the reached path at the maximum tensile shear force decreases with the tool diameter.

Unlike the mechanical loadability, which are negatively affected by the tool diameter downscaling, Figure 19 shows that similar joint interfaces could be achieved with different scaled tool diameters while the process parameters are compensated accordingly. The microsections of the welds achieved at a circumferential speed of 2513.3 mm/min and a surface pressure of 76.4 N/mm^2 exhibit weld areas with a thin diffusion layer with a thickness of around 20 µm. Overall, the results show that while using suitable parameter sets, reliable weld quality can be achieved with scaled tools within similar process time.

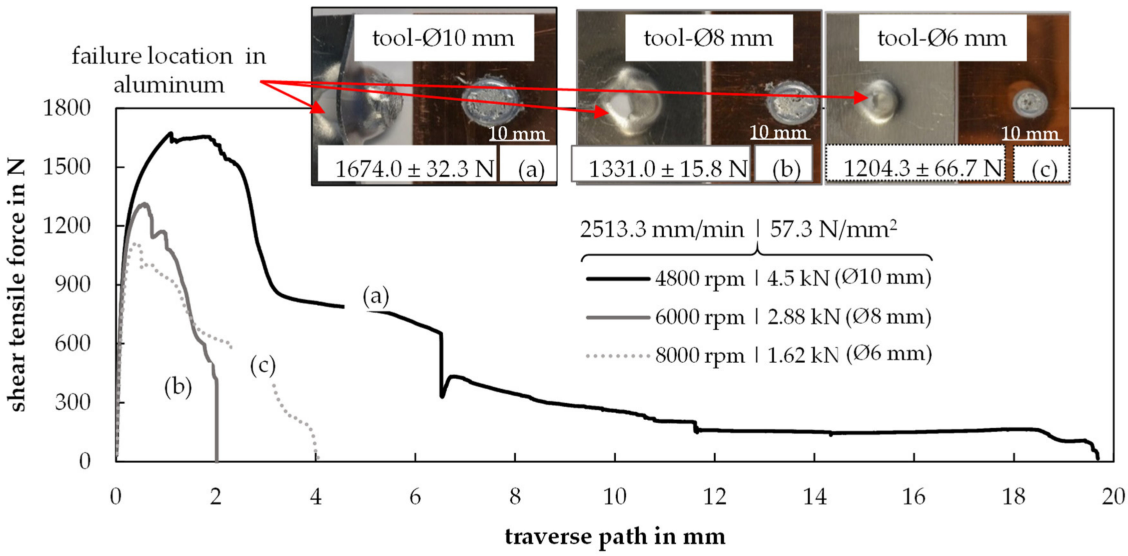

Figure 18. Effects of tool downscaling on the force-path curves and failure patterns of the welded samples.

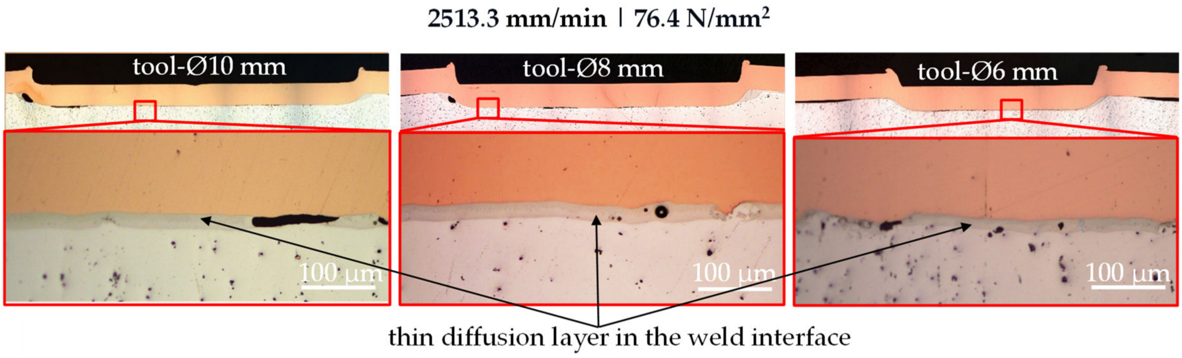

Figure 19. Microsections of joints welded with different tool diameters.

3.5. Special Aspect of Electrical Joint Properties

Apart from process-technical, the metallurgical and the mechanical aspects, electrical properties are particularly important, since the joints must be reliably current-carrying. For the electrical investigations a best-fit parameter set (2513.3 mm/min, 57.3 N/mm^2) was selected from the second quadrant (cf. Figure 17), where welds with sufficient quality at all scaling levels—that means with all tool diameters (10 mm, 8 mm and 6 mm) were achieved. The electrical resistances were gained using a 4-wire resistance measurement setup as described above (cf. Section 2.). Prior to the real measurements, a test equipment capability was carried out to evaluate the accuracy of the equipment. Different measurement tips were tested, and a torsion spring measuring tip was identified as most suitable. This delivers results with very low standard deviations ($\leq$3%).

The electrical joint properties at the different tool scaling levels are shown in Figure 20. It is obvious that the electrical resistance of the joints increases with smaller tool diameter. This was expected because of the reduced current-carrying joining area resulting in the formation of constriction resistance areas in the joints. Since low electrical resistances (i.e., high electrical conductivity) are targeted in current-carrying applications, further samples were joint with two spots using the 8 mm diameter tool (cf. Figure 20). This approach aims to enhance the mechanical properties while pursuing the process forces reduction by mean of tool diameter downscaling. The lowest electrical resistance—that means the best electrical conductivity was observed with two-spot joints as expected. Furthermore, an increase of shear tensile failure loads can be expected with the latter mentioned joint configuration.

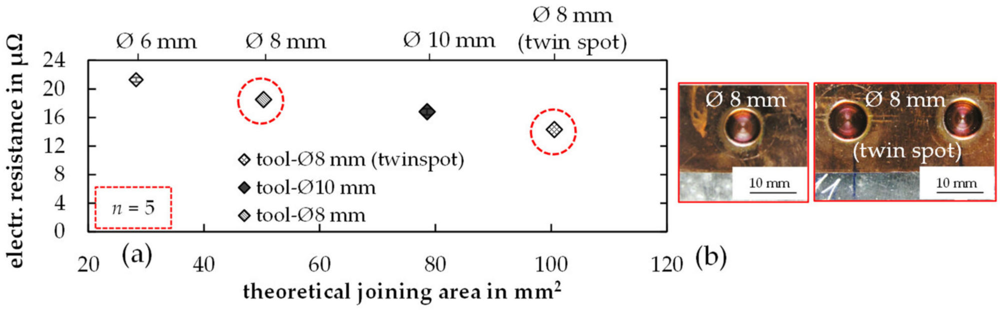

Figure 20. Effects of tool diameter downscaling on electrical properties (**a**) and sample with an 8 mm diameter spot and twin spot (**b**) exemplary. Increase of electrical resistance—i.e., decrease of electrical performance while scaling down the tool diameter—best electrical joint performance with twin spot.

4. Conclusions

The pinless friction stir spot welding is driven by the main process parameters force and rotational speed, which is responsible for the needed heat generation and surface pressure. Within the scope of this study, the process force reduction by means of tool diameter downscaling was pursued while welding thin sheets ($\leq$1 mm thickness) of pure aluminum with pure copper using the FSSW and the hybrid eutectic bonding mechanism. The used pinless tools were made of hot-working steel 1.2344. At first, a reference tool with a 10 mm diameter was used to analyze the influence of the above-mentioned main parameters on the process and on the weld quality. Especially the process time, which is particularly important on the economical aspect in the mass production and the heat propagation during the process, the weld quality, the mechanical properties as well as the electrical properties were focused. The used welding parameters were scaled on smaller tool diameters. The following insights could be gained:

- A reduction of the process time and heat propagation can be enabled using higher rotational speeds and process forces—i.e., higher surface pressure.
- Reduced process time is combined with reduced pore formation in the weld. However, high pore formation can occur at higher rotational speed despite reduced process time.
- Pore-free welds could be achieved within less than 0.5 s. The lowest process time reached in the scope of this investigation was 0.42 s $\pm$ 0.12 s.
- The results achieved with the reference tool diameter of 10 mm could be transferred on two smaller tool diameters (8 mm and 6 mm) while keeping the surface pressure and the circumferential speed constant, reducing the process force by 36% and the maximum torque occurring during the welding process by over 50%.
- The process temperature at the Al–Cu interface was constant at about 550 °C for all tool diameters, which corresponds to the eutectic temperature. Furthermore, similar heat propagation behavior was observed for the different tool diameters—i.e., the measured temperatures at the defined locations outside the welding spot were in the same range depending on the process parameter combinations.
- The welds fail predominantly in the aluminum-based material, but the welding spot is involved in the failure pattern regardless the used tool diameter. Therefore, the failure loads decrease with smaller tool diameter and thus, reduced weld area.
- The reduction of the tool diameter is combined with an increase of the electrical contact resistance—i.e., a deterioration of the electrical performance of the joint.
- Samples welded with two spots exhibit, as expected, better electrical properties than single spot welds. This is a good approach to keep the performance of current-carrying joints high, while reducing process forces by means of tool diameter downscaling.

In this regard, it can be stated that the reduction of process forces can open new windows towards the manufacturing of electrical contacts with sensitive joining materials. Additionally, regarding the accessibility, the tool diameter downscaling is quite valuable. Nevertheless, the joint performance must be guaranteed and if necessary, the approach of using two or more spots can be additionally pursued. Further research works should focus this aspect and analyze the occurring side effects and the needed boundary conditions. Furthermore, while using smaller tool diameters, high rotational speeds are needed and thus, this must be taken into consideration while designing suitable welding machines.

Author Contributions: Conceptualization, A.T.T. and T.K.; methodology, A.T.T., T.K. and J.P.B.; investigation, T.K. and A.T.T.; writing—original draft preparation, A.T.T.; writing—review and editing, A.T.T., M.G., T.K., J.P.B., P.B. and D.L.; supervision, J.P.B. All authors have read and agreed to the published version of the manuscript.

Funding: This research received no external funding.

Institutional Review Board Statement: Not applicable.

Informed Consent Statement: Not applicable.

Data Availability Statement: Not applicable.

Conflicts of Interest: The authors declare no conflict of interest.

Abbreviations

The following abbreviations and symbols are used in this manuscript:

Abbreviation	**Description**
Al	Aluminum
Cu	Copper
FSW	Friction Stir Welding
FSSW	Friction Stir Spot Welding
HFDB	Hybrid Friction Diffusion Bonding
HFEB	Hybrid Friction Eutectic Bonding
IMCs	Intermetallic Compounds
LBW	Laser Beam Welding

Symbol	**Description**	**Unit**
D	Tool Diameter	mm
F	Process Force	kN
i	Tool Diameter Index	-
n	Rotational Speed	rpm
n	Number of samples	-
p	Surface Pressure	N/mm^2
v	Circumferential Speed	mm/min
r α	Alpha	-
θ	Theta	-

References

1. Rodt, S.; Georgi, B.; Huckestein, B.; Mönch, L.; Herbener, R.; Jahn, H.; Koppe, K.; Lindmaier, J. *CO_2-Emissionsminderung im Verkehr in Deutschland: Mögliche Maßnahmen und ihre Minderungspotenziale. Ein Sachstandsbericht des Umweltbundesamtes*; Umweltbundesamt: Dessau-Roßlau, Germany, 2010. Available online: https://www.umweltbundesamt.de/publikationen/co2-emissionsminderung-im-verkehr-in-deutschland?anfrage=Kennummer&Suchwort=3773 (accessed on 25 November 2021).
2. Europäische Kommission. Vorschlag für eine Verordnung des Europäischen Parlaments und des Rates zur Schaffung des Rahmens für Die Verwirklichung der Klimaneutralität und zur Änderung der Verordnung (EU) 2018/1999 (Europäisches Klimagesetz). 2020. Available online: https://eur-lex.europa.eu/legal-content/DE/TXT/?uri=CELEX:52020PC0080 (accessed on 25 November 2021).
3. Verordnung (EG) Nr. 443/2009 des Europäischen Parlaments und des Rates zur Festsetzung von Emissionsnormen für Neue Personenkraftwagen im Rahmen des Gesamtkonzepts der Gemeinschaft zur Verringerung der CO_2-Emissionen von Personenkraftwagen und Leichten Nutzfahrzeugen. 2009. Available online: https://www.bmwi.de/Redaktion/DE/Downloads/V/verordnung-zur-festsetzung-von-emissionsnormen.html (accessed on 25 November 2021).
4. Das, A.; Li, D.; Williams, D.; Greenwood, D. Joining Technologies for Automotive Battery Systems Manufacturing. *World Electr. Veh. J.* **2018**, *9*, 22. [CrossRef]
5. Bonnekessel, S. Produktion von Li-Ionen-Akkus für Nutzfahrzeuge: Förderprojekt FUEL–Wirtschaftlicher Serienproduktionsprozesses für Nfz-Energiespeichersysteme. *WT Werkstattstech. Online* **2011**, *101*, 449–455.

6. Das, A.; Li, D.; Williams, D.; Greenwood, D. Weldability and shear strength feasibility study for automotive electric vehicle battery tab interconnects. *J. Braz. Soc. Mech. Sci. Eng.* **2019**, *41*, 54. [CrossRef]
7. Zwicker, M.F.R.; Moghadam, M.; Zhang, W.; Nielsen, C.V. Automotive battery pack manufacturing – a review of battery to tab joining. *J. Adv. Join. Process.* **2020**, *1*, 100017. [CrossRef]
8. Kalich, J.; Schlegel, S.; Füssel, U.; Großmann, S. Clinchen von Kupferwerkstoffen zur Kontaktierung elektrischer Leiter. *Metall* **2019**, *73*, 456–459.
9. Braunovic, M. Effect of connection design on the contact resistance of high power overlapping bolted joints. In Proceedings of the Forth-Seventh IEEE Holm Conference on Electrical Contacts (IEEE Cat. No.01CH37192), Montreal, QC, Canada, 10–12 September 2001; pp. 220–229, ISBN 0-7803-6667-0.
10. Lee, S.; Kim, T.; Hu, S.; Cai, W.; Abell, J. Joining Technologies for Automotive Lithium-Ion Battery Manufacturing: A Review. In Proceedings of the ASME 2010 International Manufacturing Science and Engineering Conference, MSEC 2010, Erie, PA, USA, 12–15 October 2010; Volume 1, pp. 541–549. [CrossRef]
11. Schmalen, P.; Plapper, P.; Cai, W. Process Robustness of Laser Braze-Welded Al/Cu Connectors. *SAE Int. J. Alt. Power.* **2016**, *5*, 195–204. [CrossRef]
12. Schmidt, P.A. Laserstrahlschweißen Elektrischer Kontakte von Lithium-Ionen-Batterien in Elektro-und Hybridfahrzeugen. Ph.D. Thesis, Technische Universität München, Munich, Germany, 2015.
13. Bergmann, J.P.; Petzoldt, F.; Schneider, S. Einfluss intermetallischer Phasen auf die Langzeitstabilität von Kupfer-Aluminium-Kontakten. In *Thüringer Werkstofftag 2013: Werkstoffe-Wissenschaft-Wirtschaft*; Schaaf, P., Ed.; University-Verl. Ilmenau: Ilmenau, Germany, 2013; pp. 121–126, ISBN 978-3-86360-080-8.
14. Pfeifer, S. Einfluss Intermetallischer Phasen der Systeme Al-Cu und Al-Ag auf den Widerstand Stromtragender Verbindungen im Temperaturbereich von 90 °C bis 200 °C. Ph.D. Thesis, Technischen Universität Dresden, Dresden, Germany, 2016. Available online: https://d-nb.info/1121474446/34 (accessed on 25 November 2021).
15. Leitz, A. Laserstrahlschweißen von Kupfer- und Aluminiumwerkstoffen in Mischverbindung. Ph.D. Thesis, Universität Stuttgart, Stuttgart, Germany, 2015. Available online: https://www.ifsw.uni-stuttgart.de/dokumente/dissertationen_und_habilitationen/dissertationen/Leitz_978-3-8316-7204-2.pdf (accessed on 25 November 2021).
16. Bethke, U.; Päthe, D.; Trösken, F.; Zopf, P. Laserstrahlschweißen verzinkter Bleche Einfluß von Fügespalt und Zinkschichtdicke. In *Laser in der Technik/Laser in Engineering*; Waidelich, W., Ed.; Springer: Berlin/Heidelberg, Germany, 1994; pp. 542–545, ISBN 978-3-540-57444-6.
17. Patschger, A. Grundlegende Untersuchungen zum Prozessverständnis des Laserstrahl-Mikroschweißens von Metallischen Folien. Ph.D. Thesis, Technische Universität Ilmenau, Ilmenau, Germany, 2016.
18. Zhang, Z.; Wang, K.; Li, J.; Yu, Q.; Cai, W. Investigation of Interfacial Layer for Ultrasonic Spot Welded Aluminum to Copper Joints. *Sci. Rep.* **2017**, *7*, 12505. [CrossRef] [PubMed]
19. Köhler, T.; Grätzel, M.; Bergmann, J.P. Influence of different Ni coatings on the long-term behavior of ultrasonic welded EN AW 1370 cable/EN CW 004A arrestor dissimilar joints. *Weld World* **2021**, *65*, 429–440. [CrossRef]
20. Mubiayi, M.P.; Akinlabi, E.T.; Makhatha, M.E. (Eds.) *Current Trends in Friction Stir Welding (FSW) and Friction Stir Spot Welding (FSSW)*; Springer International Publishing: Cham, Switzerland, 2019; ISBN 978-3-319-92749-7.
21. Köhler, T.; Schiele, M.; Glaser, M.; Schricker, K.; Bergmann, J.P.; Augsburg, K. In-situ monitoring of hybrid friction diffusion bonded EN AW 1050/EN CW 004A lap joints using artificial neural nets. *Proc. Inst. Mech. Eng. Part L J. Mater. Des. Appl.* **2020**, *234*, 766–785. [CrossRef]
22. Bergmann, J.P.; Petzoldt, F.; Schürer, R.; Schneider, S. Solid-state welding of aluminum to copper—Case studies. *Weld World* **2013**, *57*, 541–550. [CrossRef]
23. Genevois, C.; Girard, M.; Huneau, B.; Sauvage, X.; Racineux, G. Interfacial Reaction during Friction Stir Welding of Al and Cu. *Metall. Mater. Trans. A* **2011**, *42*, 2290. [CrossRef]
24. Mukuna Patrick, M.; Akinlabi, E. Characterization of the intermetallic compounds in aluminium and copper friction stir spot welds. *Mater. Today Proc.* **2017**, *4*, 533–540. [CrossRef]
25. Sharma, N.; Siddiquee, A.; Khan, Z. Friction stir welding of aluminum to copper—An overview. *Trans. Nonferrous Met. Soc. China* **2017**, *27*, 2113–2136. [CrossRef]
26. Sun, H.; Zhou, Q.; Zhu, J.; Peng, Y. Analysis on the Fracture of Al-Cu Dissimilar Materials Friction Stir Welding Lap Joint. *J. Mater. Eng. Perform.* **2017**, *26*, 5715–5722. [CrossRef]
27. Krutzlinger, M.; Marstatt, R.; Butzhammer, A.; Haider, F.; Zaeh, M.F. Towards an understanding of joining mechanisms of dissimilar Friction Stir Welds. In Proceedings of the 11th International Symposium on Friction Stir Welding, Cambridge, UK, 17–19 May 2016.
28. Marstatt, R.; Krutzlinger, M.; Luderschmid, J.; Constanzi, G.; Mueller, J.F.J.; Haider, F.; Zaeh, M.F. Intermetallic layers in temperature controlled Friction Stir Welding of dissimilar Al-Cu-joints. *IOP Conf. Ser. Mater. Sci. Eng.* **2018**, *373*, 12017. [CrossRef]
29. Marstatt, R.; Krutzlinger, M.; Luderschmid, J.; Zaeh, M.F.; Haider, F. Formation of a diffusion-based intermetallic interface layer in friction stir welded dissimilar Al-Cu lap joints. *IOP Conf. Ser. Mater. Sci. Eng.* **2017**, *181*, 12002. [CrossRef]
30. Osman, N.; Sajuri, Z.; Baghdadi, A.; Omar, M. Effect of Process Parameters on Interfacial Bonding Properties of Aluminium–Copper Clad Sheet Processed by Multi-Pass Friction Stir-Welding Technique. *Metals* **2019**, *9*, 1159. [CrossRef]

31. Regensburg, A.; Köhler, T.; Petzoldt, F.; Bergmann, J. Rührreibpunktschweißen von Aluminium-Kupfer-Verbindungen unter Nutzung der eutektischen Reaktion. *Metall* **2018**, *72*, 440–443.
32. Haghshenas, M.; Gerlich, A. Joining of automotive sheet materials by friction-based welding methods: A review. *Eng. Sci. Technol. Int. J.* **2018**, *21*, 130–148. [CrossRef]
33. Lakshmi Balasubramaniam, G.; Boldsaikhan, E.; Fukada, S.; Fujimoto, M.; Kamimuki, K. Effects of Refill Friction Stir Spot Weld Spacing and Edge Margin on Mechanical Properties of Multi-Spot-Welded Panels. *JMMP* **2020**, *4*, 55. [CrossRef]
34. Suhuddin, U.; Gera, D.; Alcantara, N.; dos Santos, J. Welding Multilayer Materials by Refill Friction Stir Spot Welding. In *Friction Stir Welding and Processing X*; Hovanski, Y., Mishra, R., Sato, Y., Upadhyay, P., Yan, D., Eds.; Springer International Publishing: Cham, Switzerland, 2019; pp. 245–253. ISBN 978-3-030-05751-0.
35. Briskham, P.; Blundell, N.; Han, L.; Hewitt, R.; Young, K.; Boomer, D. *Comparison of Self-Pierce Riveting, Resistance Spot Welding and Spot Friction Joining for Aluminium Automotive Sheet*; SAE Technical Paper Series; SAE International400 Commonwealth Drive: Warrendale, PA, USA, 2006.
36. Li, M.; Zhang, C.; Wang, D.; Zhou, L.; Wellmann, D.; Tian, Y. Friction Stir Spot Welding of Aluminum and Copper: A Review. *Materials* **2019**, *13*, 156. [CrossRef]
37. M Eslami, N.; Harms, A.; Deringer, J.; Fricke, A.; Böhm, S. Dissimilar Friction Stir Butt Welding of Aluminum and Copper with Cross-Section Adjustment for Current-Carrying Components. *Metals* **2018**, *8*, 661. [CrossRef]
38. Mubiayi, M.P.; Akinlabi, E.T. Evolving properties of friction stir spot welds between AA1060 and commercially pure copper C11000. *Trans. Nonferrous Met. Soc. China* **2016**, *26*, 1852–1862. [CrossRef]
39. Mubiayi, M.P.; Akinlabi, E.T. Friction Stir Welding of Dissimilar Materials: An Overview. *Int. J. Mech. Ind. Sci. Eng.* **2013**, *7*, 633. [CrossRef]
40. Su, Z.-M.; Qiu, Q.-H.; Lin, P.-C. Design of Friction Stir Spot Welding Tools by Using a Novel Thermal-Mechanical Approach. *Materials* **2016**, *9*, 677. [CrossRef] [PubMed]
41. Roos, A. Grundlegende Untersuchung über ein Neues Schweißverfahren Namens HFDB (Hybrid Friction Diffusion Bonding). Ph.D. Thesis, Technische Universität Ilmenau, Ilmenau, Germany, 2010. Available online: https://www.hereon.de/imperia/md/content/hzg/zentrale_einrichtungen/bibliothek/berichte/gkss_berichte_2010/gkss_2010_7.pdf (accessed on 25 November 2021).
42. Regensburg, A.; Grätzel, M.; Schürer, R.; Hasieber, M.; Bergmann, J.P. Process Force Reduction During Robotic Friction Stir Welding of Aluminum Alloys with Reduced Tool Aspect Ratios. In *Friction Stir Welding and Processing IX*; Hovanski, Y., Mishra, R., Sato, Y., Upadhyay, P., Yan, D., Eds.; Springer International Publishing: Cham, Switzerland, 2017; pp. 277–285, ISBN 978-3-319-52382-8.
43. Grätzel, M.; Weigl, M.; Regensburg, A.; Löhn, T.; Hasieber, M.; Bergmann, J.P. Process force reduction during friction stir welding of EN AW 6060 T66 with scaled tool diameter. In *Aluminium Heat Exchanger Technologies for HVAC&R: Lectures of the 5th International Congress Taking Place in Düsseldorf on 16 to 17 May 2017*; DVS Media GmbH: Düsseldorf, Germany, 2017; pp. 6–11, ISBN 978-3-945023-98-3.
44. Grätzel, M.; Regensburg, A.; Hasieber, M.; Gerken, J.A.; Schürer, R.; Bergmann, J.P. Scaling effects during friction stir welding of aluminum alloys with reduced tool aspect ratios. *Weld World* **2019**, *63*, 337–347. [CrossRef]
45. Grätzel, M.; Hasieber, M.; Löhn, T.; Bergmann, J.P. Reduction of friction stir welding setup loadability, process forces and weld seam width by tool scaling. *Proc. Inst. Mech. Eng. Part L J. Mater. Des. Appl.* **2020**, *234*, 786–795. [CrossRef]
46. Regensburg, A. Hybrid Friction Eutectic Bonding (HFEB)–Stoffschlüssiges Fügen von Aluminium und Kupfer unter Nutzung der eutektischen Reaktion. Ph.D. Thesis, Technische Universität Ilmenau, Ilmenau, Germany, 2021.
47. *DIN EN ISO 14273:2016-11, Widerstandsschweißen_-Zerstörende Prüfung von Schweißverbindungen_ Probenmaße und Verfahren für Die Scherzugprüfung an Widerstandspunkt-, Rollennaht- und Buckelschweißungen mit Geprägten Buckeln (ISO_14273:2016)*; Deutsche Fassung EN_ISO_14273:2016; Beuth Verlag GmbH: Berlin, Germany, 2016.
48. Keithley Instruments. *Model 2182A-Nanovoltmeter Instrument Specifications*; Keithley Instruments: Cleveland, OH, USA, 2016. Available online: https://download.tek.com/document/SPEC-2182A_DEC2016.pdf (accessed on 25 November 2021).
49. Schmid, D. *Rührreibschweißen von Aluminiumlegierungen mit Stählen für die Automobilindustrie*; Utz: München, Germany, 2015; ISBN 978-3-8316-4452-0.